Journal of Power Sources 180 (2008) 612–620

Contents lists available at ScienceDirect

Journal of Power Sources

journal homepage: www.elsevier.com/locate/jpowsour

# Effect of electrolyte composition on initial cycling and impedance characteristics of lithium-ion cells☆

D.P. Abraham*, M.M. Furczon, S.-H. Kang, D.W. Dees, A.N. Jansen

*Chemical Science and Engineering Division, Argonne National Laboratory, 9700 South Cass Avenue, Argonne, IL 60439, USA*

ARTICLE INFO

*Article history:*
Received 18 December 2007
Received in revised form 6 February 2008
Accepted 7 February 2008
Available online 26 February 2008

*Keywords:*
$LiPF_6$
$LiBF_4$
LiBOB
$LiF_2OB$
SEI
EIS

ABSTRACT

Hybrid-electric vehicles require lithium-battery electrolytes that form stable, low impedance passivation layers to protect the electrodes, while allowing rapid lithium-ion transport under high current charge/discharge pulses. In this article, we describe data acquired on cells containing $LiNi_{0.8}Co_{0.15}Al_{0.05}O_2$-based positive electrodes, graphite-based negative electrodes, and electrolytes with lithium hexafluorophosphate ($LiPF_6$), lithium tetrafluoroborate ($LiBF_4$), lithium bis(oxalato)borate (LiBOB) and lithium difluoro(oxalato) borate ($LiF_2OB$) salts. The impedance data were collected in cells containing a Li–Sn reference electrode to determine effect of electrolyte composition and testing temperature on individual electrode impedance. The full cell impedance data showed the following trend: LiBOB > $LiBF_4$ > $LiF_2OB$ > $LiPF_6$. The negative electrode impedance showed a trend similar to that of the full cell; this electrode was the main contributor to impedance in the LiBOB and $LiBF_4$ cells. The positive electrode impedance values for the $LiBF_4$, $LiF_2OB$, and $LiPF_6$ cells were comparable; the values were somewhat higher for the LiBOB cell. Cycling and impedance data were also obtained for cells containing additions of $LiBF_4$, LiBOB, $LiF_2OB$, and vinylene carbonate (VC) to the EC:EMC (3:7 by wt.) + 1.2 M $LiPF_6$ electrolyte. Our data indicate that the composition and morphology of the graphite SEI formed during the first lithiation cycle is an important determinant of the negative electrode impedance, and hence full cell impedance.



## 1. Introduction

Recent advances in cathode and anode materials have refocused attention on electrolytes as the technological bottleneck limiting the operation and performance of lithium-battery systems. Whereas, attributes such as cell potential and energy density are related to the intrinsic property of the positive and negative electrode materials, cell power density, calendar-life and safety are dictated by the nature and stability of the electrolyte and the electrode–electrolyte interfaces. A wide electrochemical window, wide temperature stability range, non-reactivity with the other cell components, non-toxicity, low cost, and a lithium-ion transference number approaching unity are, in general, desirable characteristics for lithium battery electrolytes [1,2]. In addition, the electrolyte should have excellent ionic conductivity to enable rapid ion transport between the electrodes, and be an electronic insulator to minimize self-discharge and prevent short-circuits within the cell. Research on electrolytes and on functional electrolyte additives to improve cell life, thermal abuse behavior and low-temperature (<0 °C) performance of high-power lithium-ion cells is being conducted at Argonne National Laboratory (Argonne) as part of DOE's advanced technology development (ATD) program [3–6]. The research is intended to spur commercialization of lithium-ion batteries for a wide range of vehicle applications, including hybrid-electric vehicles (HEVs), plug-in HEVs and battery electric vehicles (EVs).

For application in HEVs, electrolytes in lithium-ion cells must carry high current pulses under rapid discharge (vehicle acceleration) and rapid charge (vehicle braking) conditions. Furthermore, the electrolytes should form stable, low impedance passivation layers that allow ion transport while protecting the electrodes. Lithium battery electrolytes typically consist of alkyl carbonate solvents and lithium-bearing salts. The solvents are typically a mixture of cyclic alkyl carbonates, such as ethylene carbonate (EC), and linear alkyl carbonates, such as ethyl methyl carbonate (EMC). The highly polar (high dielectric constant) cyclic carbonates enable the dissolution of salts to sufficient concentrations, but are rather viscous. The linear carbonates, on the other hand, are weakly polar (low dielectric constant) but their low viscosity promotes rapid ion transport. The lithium-bearing salts need to dissolve in sufficient quantities

☆ The submitted manuscript has been created by the University of Chicago as Operator of Argonne National Laboratory ("Argonne") under Contract No. DE-AC02-06CH11357 with the U.S. Department of Energy. The U.S. Government retains for itself, and others acting on its behalf, a paid-up, nonexclusive, irrevocable worldwide license in said article to reproduce, prepare derivative works, distribute copies to the public, and perform publicly and display publicly, by or on behalf of the Government.

* Corresponding author. Tel.: +1 630 252 4332; fax: +1 630 972 4406.
*E-mail address:* abraham@cmt.anl.gov (D.P. Abraham).

0378-7753/$ – see front matter © 2008 Elsevier B.V. All rights reserved.
doi:10.1016/j.jpowsour.2008.02.047

**Table 1**
Electrode composition and constitution

| Positive electrode | Negative electrode |
|---|---|
| 84 wt.% $LiNi_{0.8}Co_{0.15}Al_{0.05}O_2$ (Fuji CA1505) | 92 wt.% MAG-10 graphite (Hitachi) |
| 8 wt.% PVdF binder (Kureha KF-1100) | 8 wt.% PVdF binder (Kureha #C) |
| 4 wt.% SFG-6 graphite (Timical) | |
| 4 wt.% carbon black (Chevron) | |
| 8 mg $cm^{-2}$ loading density | 4.9 mg $cm^{-2}$ loading density |
| 35-μm-thick coating | 35-μm-thick coating |
| 30-μm-thick Al current collector | 18-μm-thick Cu current collector |

and dissociate completely in the solvent; the solvated lithium-ions should be highly mobile to limit concentration polarization at the electrodes. In addition, the salt anion should be inert to electrolyte solvents and stable against oxidative decomposition at the positive electrode. Lithium hexafluorophosphate ($LiPF_6$) is the salt of choice for most lithium-ion cells because of its high solubility and excellent conductivity in alkyl carbonate solvents, and ability to form stable electrode passivation layers. Other salts under consideration at Argonne, because of their unique properties, include lithium tetrafluoroborate ($LiBF_4$), lithium bis(oxalato)borate (LiBOB) and lithium difluoro(oxalato) borate ($LiF_2OB$).

In this article we detail impedance data acquired after formation cycling on cells containing various electrolytes. The novelty of this work lies in the use of a Li–Sn reference electrode in the cells to determine effect of electrolyte composition on impedance of the positive and negative electrodes. The electrolytes studied contained alkyl carbonate solvents and $LiPF_6$, $LiBF_4$, LiBOB, and $LiF_2OB$ salts. Cells with $LiBF_4$ electrolytes have attracted renewed attention because of improved elevated temperature and low-temperature performance [7]. LiBOB- and $LiF_2OB$-based electrolytes have been in the spotlight recently because of their thermal stability, excellent ionic conductivity, and their ability to form protective solid electrolyte interphase (SEI) layers on graphite electrodes [8–15]; cells with these electrolytes show stable cycling behavior at room temperature. Because the use of electrolyte additives is known to be an effective way of improving cell performance, this article also presents data from cells containing additions of $LiBF_4$, LiBOB, $LiF_2OB$, and vinylene carbonate (VC) to the EC:EMC (3:7 by wt.) + 1.2 M $LiPF_6$ electrolyte. The effect of test temperature on cell and electrode impedance is also described. Studies of this nature are expected to influence the selection of electrolytes for use in high-power cells intended for HEV and PHEV applications.

## 2. Experimental procedure

Table 1 details the composition and constitution of electrodes employed in our cells. The positive electrode active material contained $LiNi_{0.8}Co_{0.15}Al_{0.05}O_2$ (LNCA) secondary particles, ~5–10 μm in size. The graphite particles in the negative electrode were ~10 μm in size. Table 2 lists the various electrolytes studied, and the electrolyte nomenclature employed in this article. The EC:EMC (3:7 by wt.%) solvent contained 1.2 M $LiPF_6$, 1 M $LiBF_4$, 1 M $LiF_2OB$ or 0.7 M LiBOB. These salt concentrations are typical of those being considered for our high power cells; these concentrations, typically, provide the highest electrolyte conductivity, which is important to minimize ohmic resistance in our cells. The electrolyte additive contents reflect quantities typically used to improve calendar and cycle life performance of lithium-ion cells. The $LiBF_4$, $LiF_2OB$, and LiBOB additive contents were approximately 3% of the $LiPF_6$-electrolyte weight, whereas the VC content was 1.6% of the electrolyte weight.

**Table 2**
Electrolyte nomenclature used in this article

| Composition | Nomenclature |
|---|---|
| 1.2 M $LiPF_6$ in EC:EMC (3:7, by wt.) | $LiPF_6$ |
| 1 M $LiBF_4$ in EC:EMC (3:7, by wt.) | $LiBF_4$ |
| 1 M $LiF_2BC_2O_4$ in EC:EMC (3:7, by wt.) | $LiF_2OB$ |
| 0.7 M $LiB(C_2O_4)_2$ in EC:EMC (3:7, by wt.) | LiBOB |
| 1.2 M $LiPF_6$ in EC:EMC (3:7, by wt.) + 3 wt.% $LiBF_4$ (0.4 M) | $LiBF_4$_add |
| 1.2 M $LiPF_6$ in EC:EMC (3:7, by wt.) + 3 wt.% $LiF_2BC_2O_4$ (0.26 M) | $LiF_2OB$_add |
| 1.2 M $LiPF_6$ in EC:EMC (3:7, by wt.) + 3 wt.% $LiB(C_2O_4)_2$ (0.2 M) | LiBOB_add |
| 1.2 M $LiPF_6$ in EC:EMC (3:7, by wt.) + 1.6 wt.% vinylene carbonate (0.2 M) | VC_add |

Electrochemical data were obtained both from 2032-type coin cells (1.6 $cm^2$ area electrodes) and from larger cells (32 $cm^2$ area electrodes) that incorporated a Li–Sn reference electrode. Details of the Li–Sn reference electrode preparation and cell assembly are discussed elsewhere [4,16]. The coin cells were cycled in a controlled temperature oven held at 30 °C. The reference electrode cells were assembled and tested in an inert-atmosphere glove box ($O_2$, $H_2O$ < 1 ppm) to minimize the impact of moisture and oxygen. The LNCA(+)//graphite(−) cells were cycled several times between 3 and 4.1 V, at 30 °C and ~C/12 rate, to gather information on cycling efficiencies. To shed light on electrolyte reduction behavior, complementary cycling data were also obtained in cells with graphite electrodes and lithium metal counter electrodes; these cells were typically cycled between 0 and 2 V, at 30 °C and ~C/18 rate.

All impedance data were collected on LNCA(+)//graphite(−) reference electrode cells. Electrochemical impedance spectroscopy (EIS) measurements were conducted with an EG&G 273A potentiostat and a Solartron SI1260 frequency response analyzer controlled by ZPLOT measurement software. Data for the full cell, positive electrode vs. Li–Sn, and negative electrode vs. Li–Sn were collected in the potentiostatic mode, in the 25 kHz to 10 mHz frequency range, with a 10-mV perturbation about the open-circuit voltage. The measurements were typically conducted at a full cell voltage of 3.72 V, which corresponds to 60% state-of-charge (SOC); this SOC is typically in the middle of the operating voltage window of lithium-ion cells being studied for HEV applications. At 60% SOC, the graphite electrode potential was ~80 mV vs. $Li^+$/Li. The impedance data were sequentially obtained at 30, 37, 45, and 55 °C, after allowing for ~1 h equilibration at each temperature. Cell temperature was monitored and controlled with an Omega K-series thermocouple in conjunction with an Omega CN900A Series miniature autotune temperature controller.

## 3. Results

### 3.1. Cycling and differential capacity data

Fig. 1 shows first cycle data for LNCA(+)//graphite(−) cells containing $LiPF_6$, $LiBF_4$, LiBOB and $LiF_2OB$ electrolytes. The LiBOB and $LiF_2OB$ cells show distinctive low-voltage plateaus between 1.8 and 2.0 V, which are not observed for the $LiPF_6$ and $LiBF_4$ cells. All cells show an inflection in the voltage profile around 2.8–3 V. The first cycle columbic efficiency for the cells decreased in the order $LiPF_6$ (81%) > $LiBF_4$ (77%) > LiBOB (76%) > $LiF_2OB$ (73%); the lower value for the $LiF_2OB$ cell is evidently associated with the longer low-voltage charge plateau. During the following cycles (3–4.1 V), all cells showed >98% efficiency (2nd cycle) and >99% efficiency (3rd cycle and thereafter). Fig. 2 shows differential capacity plots of the data shown in Fig. 1. The LiBOB and $LiF_2OB$ cells show peak maxima at 1.81 and 1.97 V, respectively, corresponding to the low-voltage plateaus seen in Fig. 1; the area under the peak is clearly larger for the $LiF_2OB$ cell. All cells display peaks in the 2.8–3.0 V range; these peaks are clearly seen in the Fig. 2 inset, which is an expanded view showing data in the 2.4–3.2 V range. The differential capacity data also displays several peaks in the 3.3–4.1 V range during both charge and discharge.

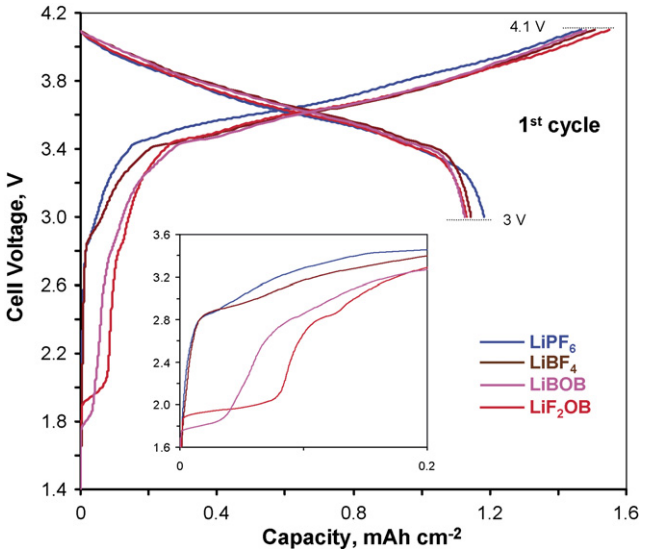


**Fig. 1.** First cycle data (30 °C) for a $LiNi_{0.8}Co_{015}Al_{0.05}O_2$(+)//graphite(−) cell at a current density of 0.1 mA $cm^{-2}$. The inset highlights the low-voltage plateaus for LiBOB and $LiF_2OB$ electrolytes.

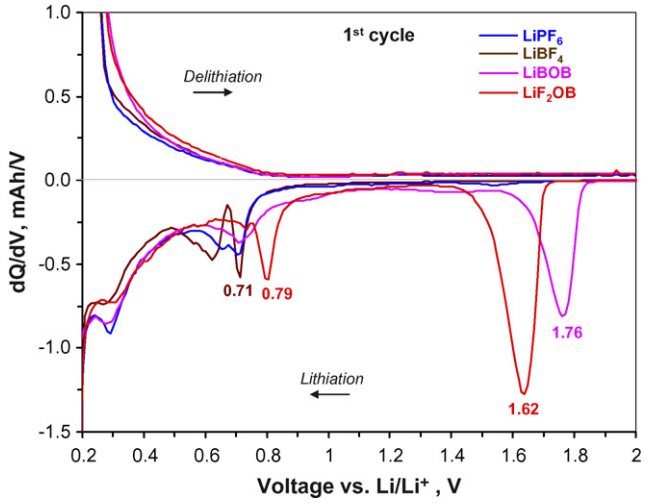


**Fig. 3.** Differential capacity plots of graphite//Li cells containing various electrolytes, cycled at 30 °C with a current density of 0.1 mA $cm^{-2}$. The *x*-axis voltage range is limited to highlight electrolyte reduction processes. The main graphite lithiation–delithiation peaks, at voltages less than ~0.2 V, are beyond the scale of this plot.

The first cycle efficiency of the LNCA(+)//graphite(−) cell is determined by various factors that include (i) limited Li-ion intercalation into the oxide particles during cell discharge at typical cycling rates because of a reduction in lithium-ion mobility resulting from a phase transition at the oxide surface [17], (ii) lithium trapped in the graphite because of potential and kinetic effects, and (iii) charge consumption at the graphite anode associated with SEI formation. In our data, the differences in first cycle efficiency are related to the graphite-SEI formation process because (i) and (ii) are determined by characteristics of the electrode active materials, which were the same in all our cells. These differences, arising from electrolyte reduction processes, can be seen in Fig. 3 that contains differential capacity data from graphite//Li cells.

In Fig. 3, the LiBOB and $LiF_2OB$ cells show peak maxima at 1.76 and 1.62 V, respectively, which are not observed for the $LiPF_6$ and $LiBF_4$ cells. It is evident that the area under the $LiF_2OB$ cell peak is larger than that of the LiBOB cell peak. These peaks are observed only in the first graphite–lithiation cycle data, even when the cells are cycled in a limited voltage range (2–1.4 V), i.e., the peaks are associated with a component (or impurity) in the LiBOB and $LiF_2OB$ salts that is reduced (and apparently consumed) early on in the first lithiation cycle. In Fig. 3, all cells show peaks in the ~0.6–0.8 V range corresponding to solvent reduction on the graphite negative electrode; these peaks are also observed only during the first graphite–lithiation cycle apparently because of the self-limiting nature of SEI growth on graphite. By accounting for the charge moved through the cells we could correlate the 1.76 V (LiBOB) and the 1.62 V ($LiF_2OB$) peaks in the graphite//Li cell data (Fig. 3) to the 1.81 V (LiBOB) and 1.97 V ($LiF_2OB$) peaks in the LNCA(+)//graphite(−) cell data (Fig. 2). Furthermore, the ~0.6–0.8 V peaks in the graphite//Li cell data are kin to the ~2.8–3 V peaks in the LNCA(+)//graphite(−) cell data. That is, peaks at voltages less than ~3.2 V in Fig. 2 are related to electrolyte reduction processes at the graphite negative electrode; subtle differences in these data indicate differences in the SEI formation processes for the various electrolytes (see Fig. 2 inset and Fig. 3). The differential capacity data peaks in the 3.3–4.1 V range are mainly associated with lithium intercalation–deintercalation processes in the electrode active materials.

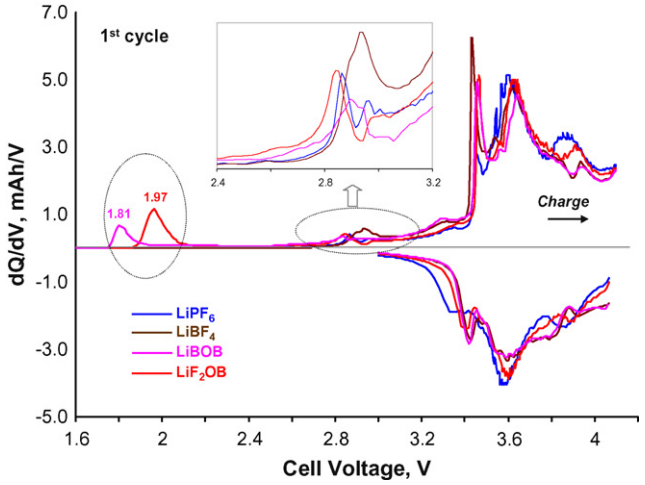


**Fig. 2.** Differential capacity plots of data shown in Fig. 1. The LiBOB and $LiF_2OB$ cells show low-voltage peak maxima at 1.81 and 1.97 V, respectively. All cells display peaks in the 2.8–3.0 V range, which are seen clearly in the inset plot. Several peaks are observed between 3.3 and 4.1 V both on charge and discharge.

Similar conclusions were drawn from data (not shown) obtained from LNCA(+)//graphite(−) cells with electrolyte additives. The LiBOB_add and $LiF_2OB$_add cells displayed low-voltage peak maxima at ~1.83 and 2.0 V in differential capacity plots, which were not observed in the other additive-cells. The areas under these low-voltage peaks for the LiBOB_add and $LiF_2OB$_add cells were smaller than the corresponding areas for the LiBOB and $LiF_2OB$ cells, which is in accordance with lower LiBOB- and $LiF_2OB$-salt concentrations of the additive cells. All cells displayed peaks in the 2.8–3.0 V range corresponding to electrolyte reduction on the graphite electrode, and peaks in the 3.3–4.1 V range associated with lithium intercalation–deintercalation processes in the electrode active materials. The differences in reduction processes because of the various electrolyte additives is displayed in Fig. 4, which contains differential capacity data from graphite//Li cells; the LiBOB_add and $LiF_2OB$_add cells show peak maxima at ~1.74 and 1.62 V, which are not seen for the other additive cells. All additive cells show peaks in the ~0.6–0.8 V range, i.e., the prior reduction of the additives does not prevent solvent reduction on the graphite negative electrode; subtle differences in these data indicate differences in SEI formation processes in the various electrolytes.

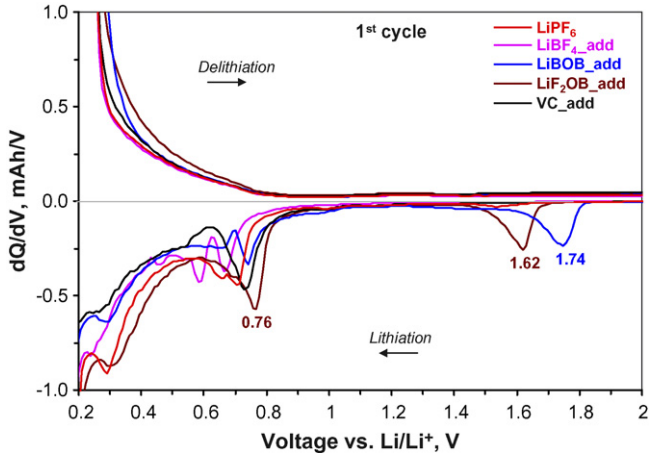


**Fig. 4.** Differential capacity plots of graphite//Li cells, containing various electrolyte additives, cycled at 30 °C with a current density of 0.1 mA cm$^{-2}$. The $LiPF_6$ cell data is shown for comparison. The *x*-axis voltage range is limited to highlight electrolyte reduction processes. The main graphite lithiation–delithiation peaks, at voltages less than ~0.2 V, are beyond the scale of this plot.

### 3.2. Impedance data

Fig. 5 shows impedance data obtained on the full cell, and on individual positive and negative electrodes from cells containing various electrolytes; the area specific impedance (in Ω-cm$^2$) data are based on the geometric area (32 cm$^2$) of the electrodes. Each dataset shows (a) a high-frequency tail (>1 kHz) that is a spurious capacitive effect arising from interaction of the measuring instrumentation with the low-impedance cell, (b) a mid-frequency arc, at frequencies between ~1 kHz and ~1 Hz, related to electrode–electrolyte interfacial processes, and (c) a low-frequency sloping line (Warburg tail), at frequencies less than ~1 Hz, mainly related to diffusion processes in the electrolyte and through the active material particles. The frequency at which the mid-frequency arc intersects the Warburg tail, $f_{min}$, is a good demarcation between the speed of the interfacial and diffusion processes and provides a relative estimate of electrode–electrolyte interfacial kinetics for the various cells.

It is evident that full cell impedance decreases in the following order: LiBOB > $LiBF_4$ > $LiF_2OB$ > $LiPF_6$. In addition, the negative electrode impedance shows a trend similar to that of the full cell, i.e., the graphite impedance is highest for the LiBOB cell and lowest for the $LiPF_6$ cell. Furthermore, the main effect in the LiBOB and $LiBF_4$ cells is seen in the mid-frequency arc, which indicates an impedance increase at the graphite electrode–electrolyte interface. The positive electrode impedances are similar for the $LiBF_4$, $LiF_2OB$, and $LiPF_6$ cells, and somewhat higher for the LiBOB cell. It is clear from Fig. 5 that, in the LiBOB and $LiBF_4$ cells, the negative electrode is the dominant contributor to full cell impedance; in the $LiF_2OB$ and $LiPF_6$ cells the full cell impedance data contains comparable contributions from both electrodes. It is interesting to note that the $LiF_2OB$ salt, which is a fluorinated version of LiBOB, produces impedance data that is similar to that of $LiPF_6$ and significantly lower than that of LiBOB.

Figs. 6–9 contain EIS data from the full cell, and positive and negative electrodes from cells containing additives to the $LiPF_6$ electrolyte. Fig. 6 shows that the impedance of the $LiBF_4$_add cell is between that of the $LiPF_6$ and $LiBF_4$ cells. In addition, the impedance increase that results from $LiBF_4$ addition is seen on the negative electrode; the impedance changes at the positive electrode are negligible. The addition of LiBOB to the $LiPF_6$-based electrolyte produced similar trends. In Fig. 7, impedance of the LiBOB_add cell is between that of the $LiPF_6$ and LiBOB cells. The LiBOB addition produces an impedance increase, especially at the negative electrode. Lower LiBOB-additive concentrations produced a smaller increase, i.e., cell impedance showed a distinct dependence on additive content, which is consistent with the data reported by Lu et al. [18]. The impedance change on $LiF_2OB$ addition to the $LiPF_6$-based electrolyte is very small (see Fig. 8) and within the margin of our experimental uncertainty. Impedance increase is only marginally larger on the addition of 1.6 wt.% VC to the $LiPF_6$-based electrolyte (Fig. 9); a small impedance increase is observed at the negative electrode. Another cell with 0.5 wt.% VC addition showed impedance data that were indistinguishable from the $LiPF_6$ cell data, i.e., smaller VC-additive concentrations barely affect cell impedance. The effect of additives to the $LiPF_6$-based electrolyte is summarized in Fig. 10. It is evident that the $LiBF_4$_add and LiBOB_add cells show the highest impedance, whereas the $LiF_2OB$_add and VC_add cells show impedances that are comparable to (or marginally larger) than that of the $LiPF_6$ cell. The LiBOB_add cell does not show the

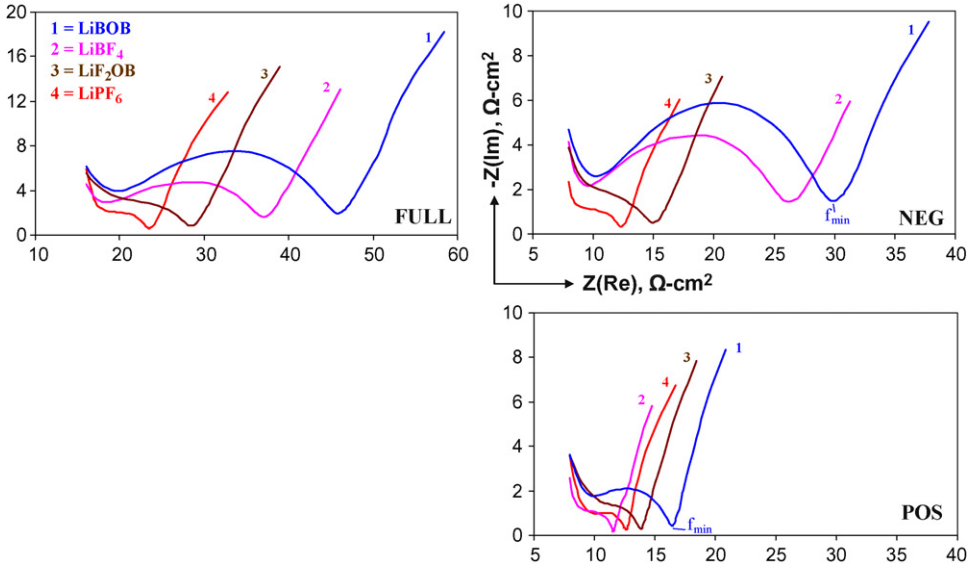


**Fig. 5.** EIS data (30 °C, 25 kHz–0.01 Hz) obtained on the full cell, and on positive and negative electrodes from cells containing various electrolytes.The data were acquired at a full cell voltage of 3.72 V. The $f_{min}$ location is indicated in the negative and positive electrode data.

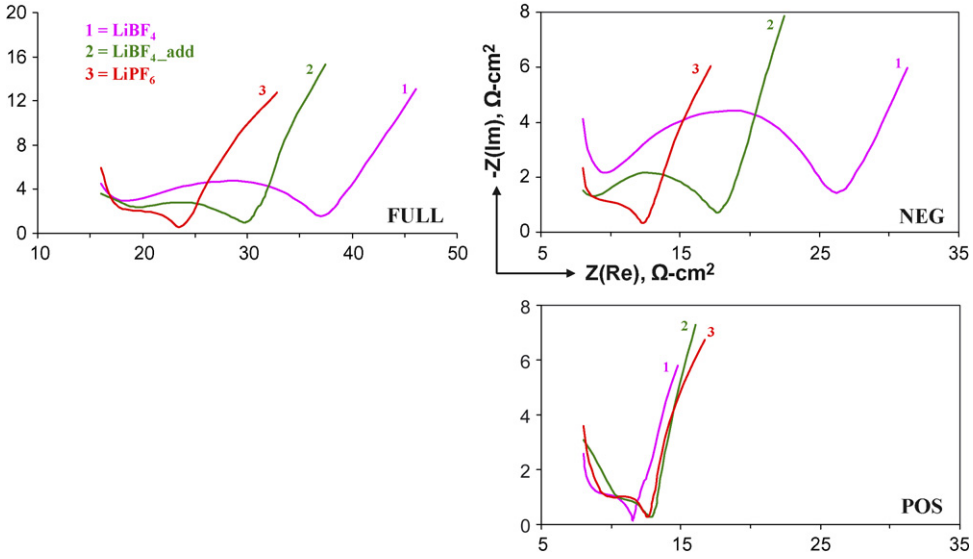


**Fig. 6.** EIS data (30 °C, 25 kHz–0.01 Hz) showing the effect of 3 wt.% LiBF4 additive on full cell, positive electrode, and negative electrode impedance. The data were acquired at a full cell voltage of 3.72 V.

highest impedance apparently because the $LiBF_4$ additive concentration (in moles) is much higher (twice) that of the LiBOB additive concentration (see Table 2).

In general, increasing the test temperature reduced impedance of all cells, which translates into higher power delivery capability at higher temperatures. Figs. 11 ($LiBF_4$ cell) and 12 (LiBOB_add cell) show representative data that display the effect of temperature on cell and electrode impedance; the trends displayed by the $LiPF_6$, LiBOB, $LiF_2OB$, $LiBF_4$_add, and VC_add cells are similar to those shown in these figures. The most significant effect of temperature is on the width of the mid-frequency impedance arc, which is smaller at the higher test temperatures, i.e., the impedance associated with the electrode–electrolyte interfacial processes decreases at higher temperatures. This decrease is typically more pronounced in the negative electrode data compared to that of the positive electrode, as seen in Figs. 11 and 12. These temperature-related effects are reversible, i.e., the data depends only on test temperature and are independent of the process (heating, cooling) by which the temperature is attained.

The improved electrode kinetics at higher temperatures is also seen in Table 3, which contains $f_{min}$ data for positive and negative electrodes in cells containing various electrolytes. The negative electrode $f_{min}$ increases by a factor of 6 between 30 and 55 °C, for the $LiPF_6$ and $LiF_2OB$ cells, and by an order of magnitude for the $LiBF_4$ and LiBOB cells. That is, the improvement in electrode kinetics is more significant for the negative electrodes that showed relative higher impedance at 30 °C. The positive electrode kinetics for the LiBOB cell also improves significantly with increasing temperature; smaller improvements are seen for the $LiPF_6$, $LiBF_4$ and $LiF_2OB$ cells. For the VC_add, $LiBF_4$_add, and LiBOB_add cells, the negative electrode kinetics improves significantly between 30 and 55 °C; the improvements in positive electrode kinetics are smaller.

In summary, the LiBOB and $LiBF_4$ cells show relatively high impedance, whereas the $LiF_2OB$ and $LiPF_6$ cells show lower impedances at 30 °C. The main contributor in the LiBOB and $LiBF_4$ cells is the negative electrode, which displays higher impedance at

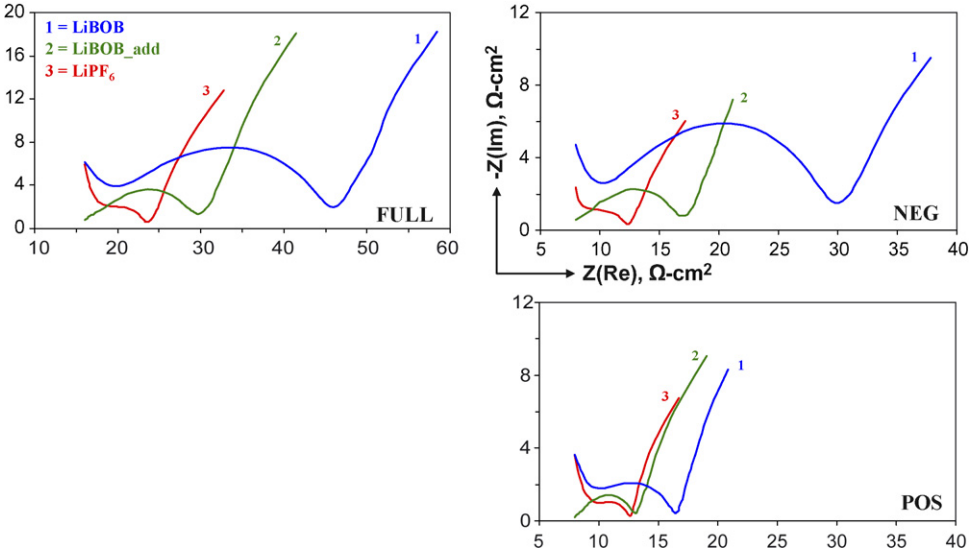


**Fig. 7.** EIS data (30 °C, 25 kHz–0.01 Hz) showing the effect of 3 wt.% LiBOB additive on full cell, positive electrode, and negative electrode impedance. The data were acquired at a full cell voltage of 3.72 V.

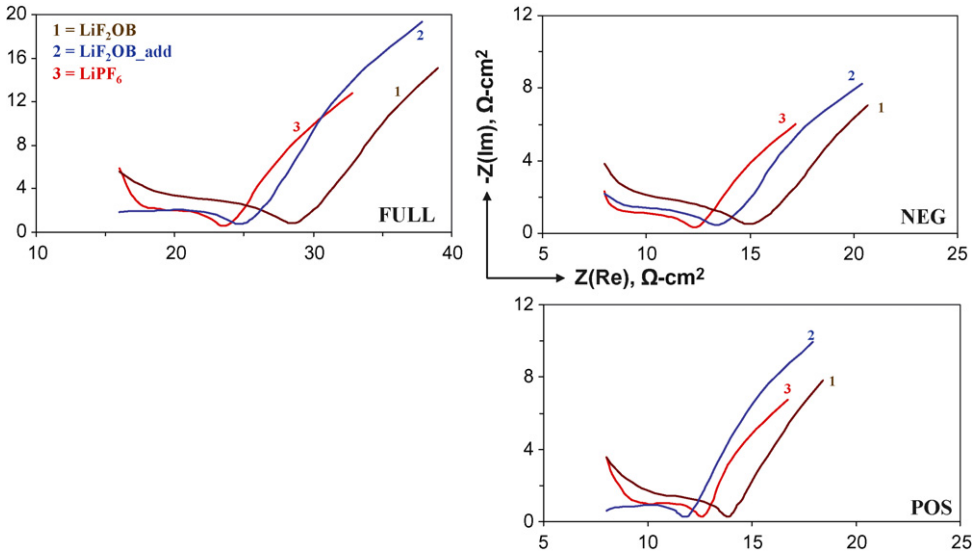


**Fig. 8.** EIS data (30 °C, 25 kHz–0.01 Hz) showing the effect of 3 wt.% $LiF_2OB$ additive on full cell, positive electrode, and negative electrode impedance. The data were acquired at a full cell voltage of 3.72 V.

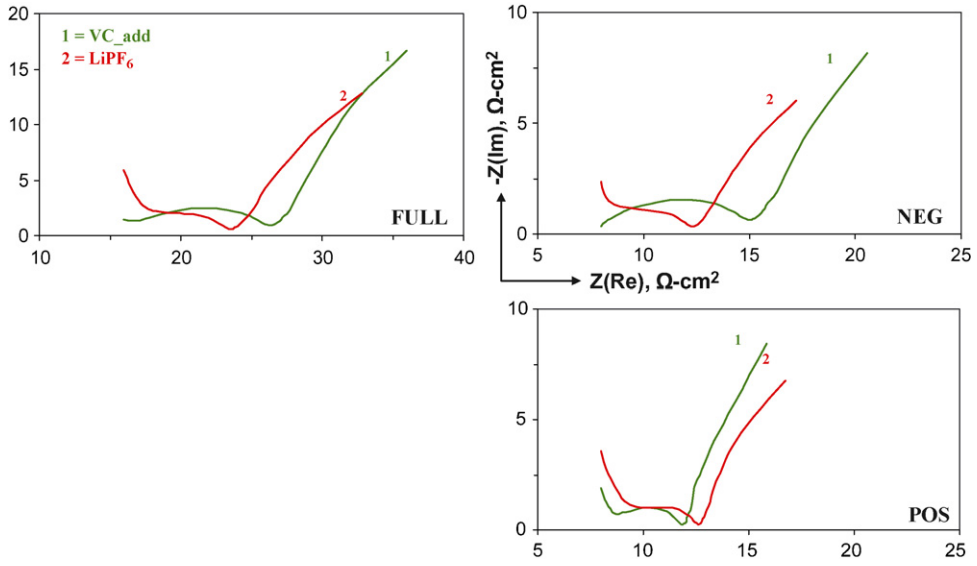


**Fig. 9.** EIS data (30 °C, 25 kHz–0.01 Hz) showing the effect of 1.6 wt.% VC additive on full cell, positive electrode, and negative electrode impedance. The data were acquired at a full cell voltage of 3.72 V.

**Table 3**
$f_{min}$ (Hz) for the positive (Pos) and negative (Neg) electrodes as a function of electrolyte composition and test temperature

| T (°C) | $LiPF_6$ | | $LiBF_4$ | | $LiF_2OB$ | | LiBOB | |
|---|---|---|---|---|---|---|---|---|
| | Pos | Neg | Pos | Neg | Pos | Neg | Pos | Neg |
| 30 | 2.5 | 4.0 | 6.3 | 0.6 | 4.0 | 4.0 | 1.6 | 0.6 |
| 37 | 4.0 | 10.0 | 6.3 | 1.0 | 6.3 | 10.0 | 4.0 | 1.6 |
| 45 | 6.3 | 15.8 | 10.0 | 2.5 | 10.0 | 15.8 | 6.3 | 2.5 |
| 55 | 10.0 | 25.1 | 15.8 | 6.3 | 10.0 | 25.1 | 15.8 | 6.3 |

| T (°C) | VC_add | | $LiBF_4$_add | | $LiF_2OB$_add | | LiBOB_add | |
|---|---|---|---|---|---|---|---|---|
| | Pos | Neg | Pos | Neg | Pos | Neg | Pos | Neg |
| 30 | 2.5 | 1.6 | 2.5 | 1.0 | 6.3 | 6.3 | 2.5 | 1.0 |
| 37 | 4.0 | 4.0 | 4.0 | 1.6 | Not Measured | | 4.0 | 2.5 |
| 45 | 6.3 | 6.3 | 4.0 | 2.5 | | | 6.3 | 6.3 |
| 55 | 10.0 | 15.8 | 6.3 | 10.0 | | | 15.8 | 15.8 |

the electrode–electrolyte interface. Higher test temperatures lower cell impedance, and especially the negative electrode impedance, in a reversible manner.

## 4. Discussion

Zhang et al. have shown that, above 10 °C, the ionic conductivity of electrolytes containing carbonate solvents and salts of interest decreases in the following order: $LiPF_6 > LiBOB > LiF_2OB > LiBF_4$ [12,13]. It is apparent that the electrolyte ionic conductivity cannot explain the observed trends in full cell impedance because the conductivity of the LiBOB electrolyte is only marginally smaller than that of the $LiPF_6$ electrolyte. In addition, the (a) differences between the positive and negative electrode data, and (b) electrode–electrolyte interfacial property changes with salt composition and test temperature, suggest that the cell impedance trends are associated with electrode surface film processes. The graphite electrode interfacial impedance, for example, arises from

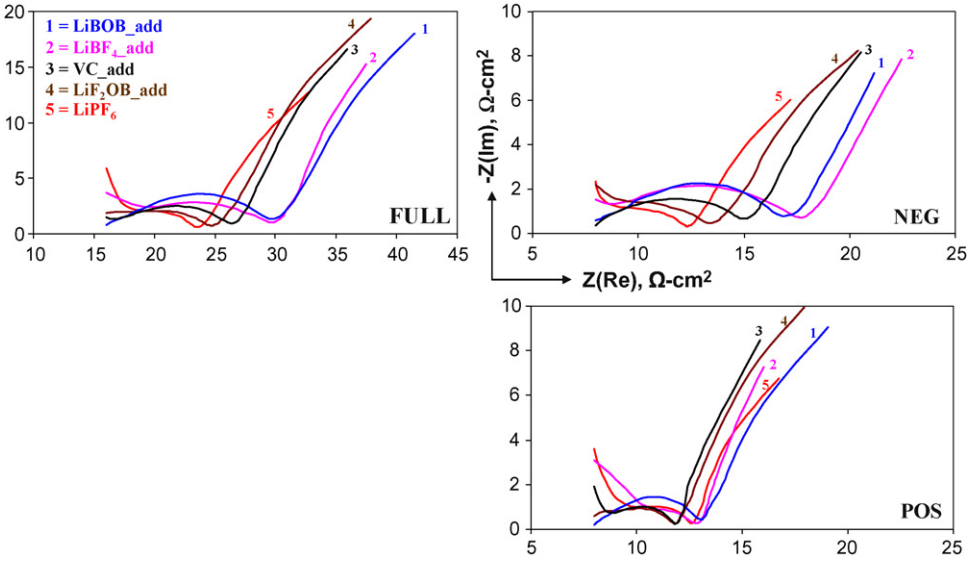


**Fig. 10.** EIS data (30 °C, 25 kHz–0.01 Hz) showing the effect of various additives to the $LiPF_6$-based electrolyte on full cell, positive electrode, and negative electrode impedance. The data were acquired at a full cell voltage of 3.72 V.

resistive, diffusive, and kinetic effects experienced by $Li^+$ during transport through micropores of the SEI before intercalation into the material, i.e., electrode impedance is governed by composition and morphology of the graphite SEI.

The nature of the graphite SEI layer after formation cycling depends on various factors that include characteristics of electrolyte solvents, composition of lithium salts, and nature of electrolyte additives. Even after decades of research, however, the SEI composition is still the subject of much debate apparently because the experimental observations depend on various factors that include graphite morphology, electrolyte purity, sample handling prior to analysis, and the analysis technique itself. There is general agreement that the SEI contains both organic and inorganic components [19–24]. In addition, the SEI layer is known to be heterogeneous along both lateral and depth dimensions. We are currently conducting graphite SEI studies in the various electrolytes examined in this study. In the meantime, our impedance data can be correlated to SEI studies conducted by other researchers.

When formed at room temperature, the graphite SEI in $LiPF_6$ electrolytes contain lithium alkyl carbonates ($ROCO_2Li$) and lithium alkoxides (ROLi) that result from solvent reduction, and LiF, $Li_xPF_y$ and $Li_xPF_yO_z$ compounds that result from salt reduction or salt decomposition [21,23]. The solvent reduction species are deposited adjacent to the graphite surface at >2.9 V full cell voltage (Fig. 2), whereas the salt-related species are formed on the electrolyte side of the interface. In a recent article, Leroy et al. showed that the graphite SEI in a $LiCoO_2$/$LiPF_6$/MCMB cell charged to 4.2 V contains ~34% LiF [24]. These significant quantities of LiF have a minor effect on graphite impedance apparently because they are not adjacent to the graphite particles. On the other hand, the graphite SEI in a $LiCoO_2$/$LiBF_4$/MCMB cell charged to 4.2 V contains only 5.4% LiF [24], but the LiF forms adjacent to the graphite particles probably because of simultaneous solvent and $LiBF_4$ reduction during early portions of the first lithiation cycle. It appears likely that the higher graphite impedance in $LiBF_4$ electrolytes results in part from LiF crystallites [25] adjacent to the graphite edge planes that impede

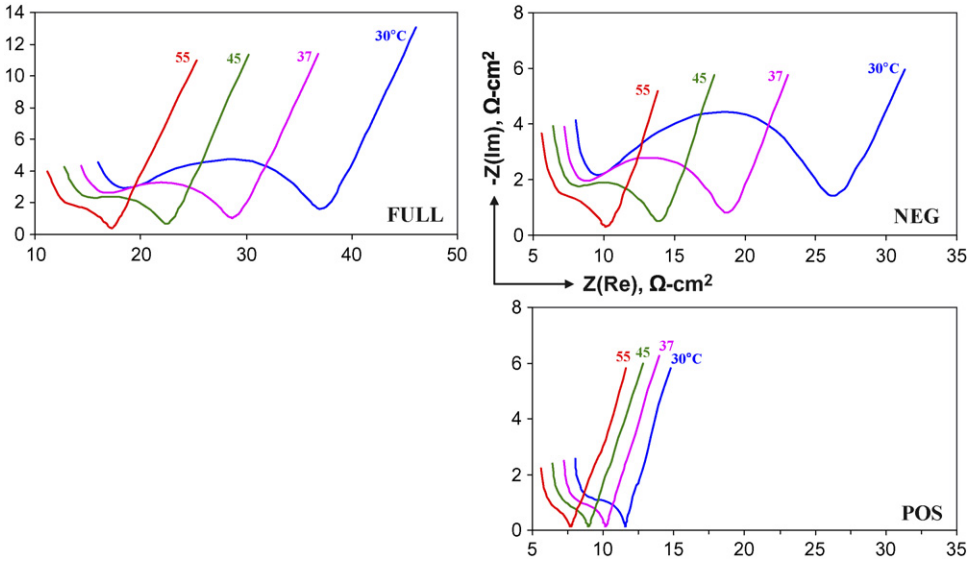


**Fig. 11.** EIS data (25 kHz–0.01 Hz) showing the effect of test temperature on full cell, positive electrode and negative electrode impedance in the cell containing the $LiBF_4$ electrolyte. The data were acquired at a full cell voltage of 3.72 V.

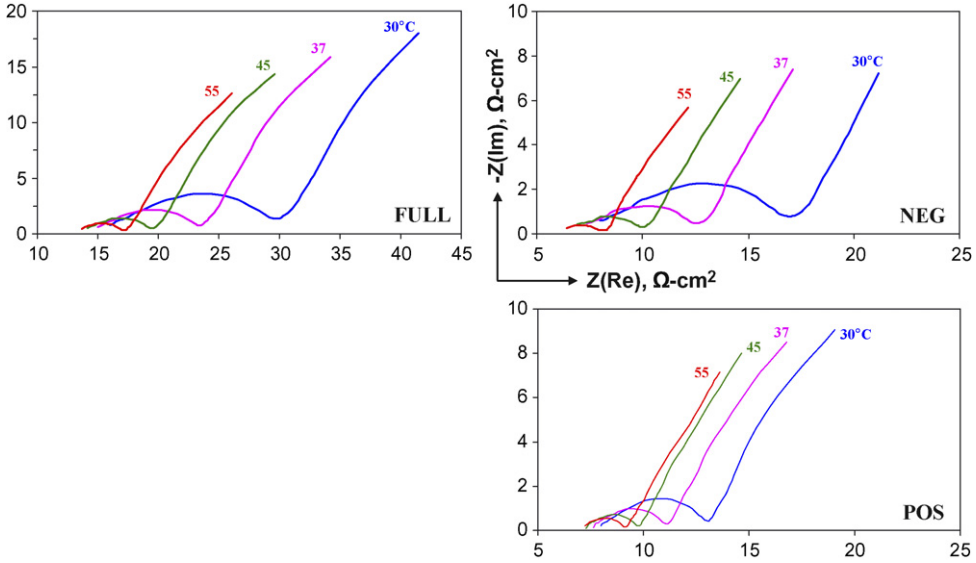


**Fig. 12.** EIS data (25 kHz–0.01 Hz) showing the effect of test temperature on full cell, positive electrode and negative electrode impedance on the LiBOB_add cell. The data were acquired at a full cell voltage of 3.72 V.

$Li^+$ motion. The intermediate impedance of the graphite electrode in the $LiBF_4$_additive cell (Fig. 6) may also be the result of a higher LiF content (along with solvent reduction species) adjacent to the active material surface.

In the LiBOB and $LiF_2OB$ cells the 1.81 and 1.97 V peaks in Fig. 2 (or the 1.76 and 1.62 V peak in Fig. 3) have been attributed to reduction of oxalate-related molecular moieties [8,14,25]; the origin of this oxalate-moiety is uncertain at this time. In graphite//Li cells containing the LiBOB salt, Wachtler et al. reported that this peak could not be eliminated even after salt purification by various techniques [8]. They concluded that the peak is probably intrinsic to LiBOB electrolytes (and by extension the $LiF_2OB$ electrolytes). Whatever be its origin the reduction products associated with this peak precipitate, at least in part, on the graphite surface. It should be noted that these reduction products (i) may attenuate further reduction processes (such as solvent reduction) for the LiBOB electrolytes, but do not attenuate further reduction for $LiF_2OB$ electrolytes (see Figs. 3 and 4), and (ii) are not solely responsible for the higher impedance of the LiBOB electrolytes because the area under the $LiF_2OB$ cell peak is larger than that of the LiBOB cell peak, as indicated previously (Fig. 3).

From studies in electrolytes containing both EC and LiBOB, Xu et al. have indicated that EC-reduction occurs before the reductive decomposition of the BOB anion [26]. Furthermore, assuming that the site-preference described by Bar-Tow et al. [27] is a universal trend, they suggested that solvent-reduction products ($ROCO_2Li$, ROLi, etc.) may show preference for the basal planes, whereas salt-reduction products (carbonyl-rich boron-bearing compounds) may show preference for the edge planes. These carbonyl-rich oligomers may be responsible for the higher graphite impedance in the LiBOB and LiBOB_additive cells because the SEI formed on graphite edge planes (the sites of lithium intercalation) is mainly responsible for impeding $Li^+$ motion. The graphite SEI in $LiF_2OB$ electrolyte is believed to contain lithium alkyl carbonates, lithium alkoxides and alkyl esters of oxalic acid (or lithium oxalate) [28]. The significantly lower graphite impedance in the $LiF_2OB$ and $LiF_2OB$_additive cells evidently reflects the effect of fluorine in modifying the SEI at the graphite edge planes. We speculate that the fluorine atoms either modify the graphite edge-sites and/or reduce oligomer chain length, thereby producing a more compact and better $Li^+$ ion conducting SEI.

The addition of VC to EC-based $LiPF_6$ electrolytes is known to improve performance of graphite anodes by reducing irreversible capacity, suppressing salt reduction, and improving cycling behavior [29–31]. The VC-additive reduces before EC producing polymeric species, such as polyvinylene carbonate and polyacetylene adjacent to the graphite surface; other VC reduction products include lithium vinylene dicarbonate $(CHOCO_2Li)_2$, lithium divinylene dicarbonate $(CH{=}CHOCO_2Li)_2$, lithium divinylene dialkoxide $(CH{=}CHOLi)_2$, and lithium carboxylate (RCOOLi) [30]. Moreover, the SEI contains less LiF [29], which forms on the electrolyte side of the interface. The dependence of graphite electrode impedance on VC content, and the marginally larger impedance of the graphite electrode with 1.6 wt% VC addition indicates that the VC-reduction products are more resistant to $Li^+$ ion transport than EC-reduction products.

The similar impedances displayed by the positive electrode in $LiPF_6$, $LiBF_4$, $LiBF_4$_add, $LiF_2OB$, $LiF_2OB$_add, and VC_add cells suggest that electrode surface films formed in these electrolytes are similar. In general, these films contain a mixture of $ROCO_2Li$, ROLi, $ROCO_2R$, LiF and oligomeric species formed by various mechanisms that include nucleophilic reactions, acid–base reactions, and induced polymerization reactions [32]. In contrast to the graphite SEI, these films are thinner and are not altered by short-term exposure to ambient air [21]. The higher impedance observed in LiBOB and LiBOB_add cells apparently reflects the modification of the positive electrode surface film by the $BOB^-$ anion; this modification is currently under investigation.

## 5. Conclusion

Initial cycling and impedance data were acquired on cells containing electrolytes comprising various salts in alkyl carbonate solvents. Several peaks were observed in the differential capacity data from the first cycle in LNCA(+)//graphite(−) cells; the peaks at voltages less than 3.1 V are related to electrolyte reduction processes at the graphite negative electrode, whereas peaks in the 3.3–4.1 V range arise from lithium intercalation–deintercalation reactions in the active materials. Full cell impedance data at 30 °C showed the following trend: LiBOB > $LiBF_4$ > $LiF_2OB$ > $LiPF_6$. Data from reference electrode cells showed that the graphite negative electrode was the main contributor to full cell impedance,

especially for the LiBOB and $LiBF_4$ cells. Furthermore, the main differences were observed in the mid-frequency arc of the EIS data, which indicated differences in the graphite–electrolyte interface, that is, in the SEI formed in various electrolytes. Cells containing LiBOB, $LiBF_4$ and VC additives displayed impedances that were larger than that of the $LiPF_6$ cell, mainly because of higher impedances at the graphite negative electrode; the $LiF_2OB$_add cell impedance was only marginally larger than that of the $LiPF_6$ cell. The impedance data show a distinct dependence on additive content, which is consistent with the data reported by previous investigators.

## Acknowledgments

This work was conducted as part of the Advanced Technology Development program, which is financially supported by the U.S. Department of Energy (DOE), Office of Vehicle Technologies. We are grateful to Gary Henriksen for programmatic support and to Dr. Khalil Amine for acquiring the various salts and additives used in this study.

## References

[1] K. Xu, Chem. Rev. 104 (2004) 4303.
[2] D. Aurbach, Y. Talyosef, B. Markovsky, E. Markevich, E. Zinigrad, L. Asraf, J.S. Gnanaraj, H.-J. Kim, Electrochim. Acta 50 (2004) 247.
[3] Z. Chen, J. Liu, K. Amine, Electrochem. Solid-State Lett. 10 (2007) A45.
[4] A.N. Jansen, D.W. Dees, D.P. Abraham, K. Amine, G.L. Henriksen, J. Power Sources 174 (2007) 373.
[5] D.P. Abraham, E.P. Roth, R. Kostecki, K. McCarthy, S. MacLaren, D.H. Doughty, J. Power Sources 161 (2006) 648.
[6] D.P. Abraham, J.L. Knuth, D.W. Dees, I. Bloom, J.P. Christophersen, J. Power Sources 170 (2007) 465.
[7] S.S. Zhang, K. Xu, T.R. Jow, J. Solid State Electrochem. 7 (2003) 147.
[8] M. Wachtler, M.W. -Mehrens, S. Ströbele, J.-C. Panitz, U. Wietelmann, J. Appl. Electrochem. 36 (2006) 1199.
[9] R. Holomb, W. Xu, H. Markusson, P. Johansson, P. Jacobsson, J. Phys. Chem. A 110 (2006) 11467.
[10] T.R. Jow, K. Xu, M.S. Ding, S.S. Zhang, J.L. Allen, K. Amine, J. Electrochem. Soc. 151 (2004) A1702.
[11] K. Xu, U. Lee, S. Zhang, M. Wood, T.R. Jow, Electrochem. Solid-State Lett. 6 (2003) A144.
[12] S.S. Zhang, K. Xu, T.R. Jow, Electrochim. Acta 51 (2006) 1636.
[13] S.S. Zhang, Electrochem. Commun. 8 (2006) 1423.
[14] S.S. Zhang, J. Power Sources 163 (2007) 713.
[15] L. Larush-Asraf, M. Biton, H. Teller, E. Zinigrad, D. Aurbach, J. Power Sources 174 (2007) 400.
[16] D.P. Abraham, S.D. Poppen, A.N. Jansen, J. Liu, D.W. Dees, Electrochim. Acta 49 (2004) 4763.
[17] J.R. Mueller-Neuhaus, R.A. Dunlap, J.R. Dahn, J. Electrochem. Soc. 147 (2000) 3598.
[18] W. Lu, Z. Chen, H. Joachin, J. Prakash, J. Liu, K. Amine, J. Power Sources 163 (2007) 1074.
[19] D. Aurbach, J. Power Sources 89 (2000) 206.
[20] E. Peled, D. Golodnitsky, C. Menachem, D. Bar-Tow, J. Electrochem. Soc. 145 (1998) 3482.
[21] A.M. Andersson, D.P. Abraham, R. Haasch, S. MacLaren, J. Liu, K. Amine, J. Electrochem. Soc. 149 (2002) A1358.
[22] M. Herstedt, D.P. Abraham, J.B. Kerr, K. Edström, Electrochim. Acta 49 (2004) 5097.
[23] S. Leroy, F. Blanchard, R. Dedryvère, H. Martinez, B. Carré, D. Lemordant, D. Gonbeau, Surf. Interf. Anal. 37 (2005) 773.
[24] S. Leroy, H. Martinez, R. Dedryvère, D. Lemordant, D. Gonbeau, Appl. Surf. Sci. 253 (2007) 4895.
[25] A.M. Andersson, H. Henningson, U. Siegbahn, K. Jansson, Edström, J. Power Sources 119–121 (2003) 522.
[26] K. Xu, U. Lee, S. Zhang, J.L. Allen, T.R. Jow, Electrochem. Solid-State Lett. 7 (2004) A273.
[27] D. Bar-Tow, E. Peled, L. Burstein, J. Electrochem. Soc. 146 (1999) 824.
[28] S.-H. Kang, D.P. Abraham, A. Xiao, B.L. Lucht, J. Power Sources 175 (2008) 526.
[29] D. Aurbach, K. Gamolsky, B. Markovsky, Y. Gofer, M. Schmidt, U. Heider, Electrochim. Acta 47 (2002) 1423.
[30] H. Ota, Y. Sakata, A. Inoue, S. Yamaguchib, J. Electrochem. Soc. 151 (2004) A1659.
[31] S.S. Zhang, J. Power Sources 162 (2006) 1379.
[32] D. Aurbach, B. Markovsky, G. Salitra, E. Markevich, Y. Talyossef, M. Koltypin, L. Nazar, B. Ellis, D. Kovacheva, J. Power Sources 165 (2007) 491.